Materials Today Energy 23 (2022) 100889

Contents lists available at ScienceDirect

Materials Today Energy

journal homepage: www.journals.elsevier.com/materials-today-energy/

Ultra-flexible and foldable gel polymer lithium−ion batteries enabling scalable production

D. Wei [a, *, g], W. Shen [b, g], T. Xu [b, g], K. Li [b], L. Yang [b], Y. Zhou [b], M. Zhong [b], F. Yang [b], X. Xu [b], Y. Wang [b], M. Zheng [b], Y. Zhang [c, d], Q. Li [c, d], Z. Yong [c], H. Li [e], Q. Wang [f]

[a] Beijing Institute of Nanoenergy and Nanosystems, Chinese Academy of Sciences, China
[b] Beijing Graphene Institute, Beijing 100094, PR China
[c] Key Laboratory of Multifunctional Nanomaterials and Smart Systems, Advanced Materials Division, Suzhou Institute of Nano-Tech and Nano-Bionics, Chinese Academy of Sciences, Suzhou 215123, China
[d] School of Nano-Tech and Nano-Bionics, University of Science and Technology of China, Hefei 230026, China
[e] State Key Laboratory of Advanced Power Transmission Technology, Global Energy Interconnection Research Institute Co. Ltd., Beijing 102211, China
[f] College of Materials Science and Engineering, Taiyuan University of Technology, Taiyuan 030024, China

ARTICLE INFO

Article history:
Received 15 July 2021
Received in revised form
24 September 2021
Accepted 26 October 2021
Available online 9 November 2021

Keywords:
Bendable batteries
Carbon nanotube
Gel polymer electrolyte
Mass production

ABSTRACT

Flexible lithium−ion batteries are an emerging and promising technology for next-generation flexible devices; however, some potential problems, such as potential safety hazards of organic liquid electrolytes, severe capacity loss caused by poor adhesion between electroactive materials and current collectors, and the unscalable production of flexible current collectors, prevent flexible batteries from being used in practice. This study demonstrates a safety reinforced ultra-flexible and foldable lithium−ion battery using $LiCoO_2$ (LCO) as the cathode, $Li_4Ti_5O_{12}$ (LTO) as the anode, a high-quality carbon nanotubes film as a flexible current collector, and a novel porous composite as the gel polymer electrolyte. The flexible battery exhibits superior electrochemical performance compared to other flexible batteries reported, with a capacity retention rate of 93% after 150,000 cycles of mechanical bending. The gravimetric energy density of the flexible electrodes is 1.6 times higher than that of standard electrodes using metal foils as current collectors. More importantly, the flexible battery offers extreme safety performance and performs very well under various severe conditions, such as repeated folding and punching. These results demonstrate the promising potential of flexible batteries for many wearable applications and offer a new platform for the scalable production of flexible and wearable energy storage technologies.

1. Introduction

Wearable energy storage devices are receiving intensive research endeavors, aiming at powering a variety of deformable functional devices such as smart clothes, electronic skins, implantable medical devices, wearable smartphones, and healthcare sensors [1–4]. Conventional energy devices, such as lithium−ion batteries (LIBs), typically appear in a rigid plate, which is unfavorable for many applications, especially in the fields of deformable functional devices which require small size, light weight, high flexibility, and foldability [5]. Therefore, the development of wearable or flexible energy storage devices is extremely important for the growing demand of flexible devices. Since their commercialization in the 1990s, LIBs have seen rapid developments. Compared to other rechargeable battery technologies, LIBs have many advantages, including relatively high energy and power densities, long cycling life, little memory effect, and low self-discharge [6–9]. When used in flexible electronics, LIBs also need to be flexible, safe, thin, stretchable, and even foldable [10,11].

To meet the demands of flexible electronics, flexible LIBs require that all of the key components (current collector, active layer, separator, and packaging) be bendable or even foldable. Conventional metal foils (Al and Cu foils) as current collectors for the positive and negative electrodes are unfit for flexible LIBs. Because such foils are stiff and subject to fatigue failures. The metal foils are difficult to restore to their original shape after deformation. Moreover, the active layer is easily delaminated from the smooth surface of metal foils when the flexible batteries are bent. In

* Corresponding author.
E-mail address: weidi@binn.cas.cn (D. Wei).
[g] D. Wei, Wei Shen and Tao Xu contributed equally to this work.

https://doi.org/10.1016/j.mtener.2021.100889
2468-6069/

addition, the heavy weight of metal foils reduces the gravimetric capacity of the whole battery system. The areal densities of Al and Cu foils are about 5.0 and 13.0 mg/cm^2 (thickness of 10–20 μm), respectively, and they account for 10–15% of the total weight of a battery [11]. Therefore, replacing the metal foils with a highly conductive, lightweight, thin, and flexible current collector could enhance both the gravimetric energy density and mechanical flexibility of LIBs [12,13]. Recently, carbon-based materials are obtained with high conductivity and low density, are chemically stable within a wide range of electrochemical voltage, and thereby are regarded as the promising choice for current collectors in flexible LIBs [10,14]. In particular, carbon nanotubes (CNTs), typical one dimensional (1D) carbon materials, have been widely explored for use as current collectors by various preparation methods, such as vacuum filtration [15,16], self-assembly [17,18], dry-drawing [19,20], blade coating [21,22], and so on. Thanks to the tremendous research efforts devoted over the past decades, research on flexible LIBs has made great progress. However, the sheet resistance of the reported carbon material current collectors is as high as 5–50 Ω/sq [23–27] Moreover, the breaking strength of carbon material current collectors is only in the 5–15 MPa range [26,28–30]. At present, the high sheet resistance and low breaking strength of carbon current collectors are far from meeting the requirements of flexible LIBs. Furthermore, research on the carbon material current collectors is still in the laboratory stage, far from the scalable production. Therefore, for future practical application, developing a flexible current collector with low sheet resistance, high breaking strength, and scalable production is urgently required.

Safety is always a critical concern for LIBs. There are huge potential safety hazards for commercialized LIBs due to employing an organic carbonate solvent and polyolefin-based separators. These potential risks (leakage, combustion, and explosion) will become even more challenging for flexible LIBs. In this case, all solid polymer electrolytes provide a promising opportunity to overcome the safety issue. However, the reported all solid polymer electrolytes mostly exhibit low ionic conductivities (10^{-8}–10^{-5} S/cm) and poor interfaces with electrodes, resulting in a deteriorated electrochemical performance [31–33]. To this end, combined with the advantages of both the liquid and solid electrolytes, gel polymer electrolytes (GPEs) have attracted increasing attention as they can function as not only electrolytes but also separators [34,35]. Moreover, the flexibility and elasticity of GPEs are also prone to tolerate the volume change of electrode materials during charge and discharge processes [36]. Therefore, GPEs have become one of the most desirable alternatives among various electrolytes for flexible LIBs. At present, the low ionic conductivity, poor mechanical strength, and narrow electrochemical window are still not satisfactory enough to meet practical needs. On the basis of this, it is essential to explore a new GPE with comprehensive performance in terms of high ionic conductivity, proper mechanical strength, superior thermal stability, wider electrochemical window, and excellent electrochemical performance.

Here we demonstrate a flexible rechargeable LIB using a flexible high-quality CNTs film as a current collector and a new porous composite GPE based on $Li_{6.4}La_3Zr_{1.4}Ta_{0.6}O_{12}$ (LLZTO) nanoparticles embedded in the poly(vinylidene fluoride-tri-fluoroethylene-chlorofluoroethylene) (PTC) matrix as the electrolyte and separator. The ultra-thin 13 μm CNTs film synthesized by the floating catalyst CVD-growth method exhibits superior mechanical strength with a breaking stress of ~82.1 MPa, which is just slightly lower than that of commercial metal foil, but significantly higher than that of carbon current collectors reported in the literature [28,29,37–43]. Moreover, the sheet resistance of the CNTs film in this study is as low as ~1.4 Ohm/sq, which is also far less than most reported carbon current collectors with the sheet resistance as high as 5–50 Ohm/sq [23–27]. The thickness of the CNTs film can be well controlled at ~13 μm, which is comparable to that of commercial metal foil. More importantly, the CNTs film still shows excellent flexibility after repeated folding in half at 180° and does not cause cracking or delamination of the active materials. Furthermore, to the best of our knowledge, LIBs using PTC-based composite GPE as a new type of material have so far been barely explored. The present work is one of the first scientific reports on safety-enhanced PTC/LLZTO composite GPEs for flexible LIBs. It was demonstrated that such porous PTC-based composite GPEs exhibit superior ionic conductivity than Celgard/liquid electrolytes and also exhibit high interface stability mainly due to the strong absorption of liquid, high thermal stability, and high electrochemical stability at a broad temperature range. Combining special properties of the CNTs film and PTC-based composite GPE, the flexible battery exhibits not only superior flexibility even after 150,000 times mechanical bending, but also high safety even under perforated conditions, indicating its promising applications for high-performance flexible energy storage devices.

2. Experimental section

2.1. Materials

PTC (Mw ≈ 400,000–600,000) was purchased from Wuhan Methyl Technology Co., Ltd. LLZTO, LCO, and LTO were supplied by Hefei Kejing Materials Technology Co., Ltd. LiTFSI was purchased from Beijing Inno Chem Science & Technology Co., Ltd. The liquid electrolyte in this study was purchased from Suzhou Duoduo Chemical Technology Co., Ltd.

2.2. Preparation of the CNTs film

The CNTs film was synthesized using the floating catalyst CVD-growth method. A solution of ethyl alcohol of absolute ethyl alcohol with 1.2 vol% ferrocene and 0.4 vol% thiophene carried by Ar/H_2 was injected at a rate of 20 mL/h into a horizontal furnace and atomized at 1,300 °C. Under these synthesis conditions, the nanotubes spontaneously formed a continuous sock-like aerogel in the gas flow, which can be blown out with the carrier gas. The CNT aerogels were continuously wound by a rotating mandrel and they were densified by in-situ liquid-spraying of an ethanol–water solution. After the evaporation of the liquid, a multilayered seamless CNTs film with a maximum width of 1 m was prepared and can be rolled into storage. The scalable production line using the floating catalyst CVD-growth method is estimated to produce about 100,000 m^2 of CNT films per year. The large-scale preparation of CNT films ensures the scalable production of flexible batteries.

2.3. Preparation of the composite gel polymer electrolyte

The porous composite GPE was synthesized using the phase inversion method. First, LiTFSI (0.1 g), LLZTO, and PTC (2.5 g) were completely dissolved in 10 mL of dimethylformamide (DMF) under ultrasonic dispersion and magnetic stirring at 30 °C. The slurry was used as a doctor-blading method cast on a clean glass plate and then transferred into an ethanol bath to produce phase inversion (ethanol molecules easily replace and occupy the position of DMF solvent molecules. It is beneficial to form a porous structure). Finally, the porous composite membrane was heated in a vacuum oven for 24 h at 80 °C. To prepare composite porous GPEs with different LLZTO contents, the samples with different mass ratios of 0, 5, 15, 25, and 40 wt% (LLZTO/(PTC + LiTFSI + LLZTO)) were prepared and denoted as P-CPE-0%, P-CPE-5%, P-CPE-15%, P-CPE-25%,

and P-CPE-40%, respectively. For comparison, the non-porous composite GPE of PTC/LiTFSI without LLZTO was also fabricated by direct drying method instead of the phase inversion method and denoted as N-GPE-0%. The as-obtained membranes were immersed into the liquid electrolyte (1.0 m $LiPF_6$ in EC/DEC = 1:1, v/v with 5.0% FEC) for 2 h, ultimately obtaining the composite GPE.

2.4. Electrochemical test for a flexible full cell

A flexible lithium−ion full cell was assembled in an Ar-filled glove box with the CNTs film as the current collector, LCO as the cathode, LTO as the anode, and composite GPE as the electrolyte and separator. As current collectors, the rolled CNT films were applied to a small LIBs production line, and the electrode materials were coated by a blade-coating machine. In the subsequent electrochemical performance test of a flexible full cell, the mass loadings of LCO and LTO were uniformly controlled at ≈5.8 and ≈4.0 mg/cm^2, respectively. For comparison, various mass loadings of electrodes were also prepared. The mass loadings of the LCO material were ≈3.6, ≈9.6, and ≈14.0 mg/cm^2, and the corresponding mass loadings of the LTO material were ≈2.5, ≈6.6, and ≈9.6 mg/cm^2, respectively. The N/P ratio (negative electrode capacity/positive electrode capacity) was ~0.8. The electrode was composed of LCO (LTO), super P (SP) as the conductive additive, and PVDF as the binder (LCO:SP:PVDF = 85:8:7 weight ratio). The electrode was dried at 80 °C in vacuum for at least 10 h. The assembled full cell was tested at different charge/discharge rates on a Land battery tester (Wuhan Land Electronic Co. Ltd.). The range of test voltage is 1.5−2.8 V.

2.5. Electrochemical evaluation

The ionic conductivities of GPEs were tested by Autolab, Metrohm via coin cell of stainless steel (SS)/GPE/SS by electrochemical impedance spectroscopy (EIS) over the frequency range of 10^{-2} Hz−10^6 Hz with an amplitude voltage of 10 mV. The ionic conductivity (σ) was evaluated from the equation:

$$\sigma = \frac{d}{S*R} \quad (1)$$

where R is the resistance value of the bulk electrolyte measured by EIS, d is the thickness of the electrolyte membrane, and S is the area of the electrode.

2.6. Characterization

The morphology and microstructure of the samples were examined by scanning electron microscopy (SEM) (FE-SEM, Zeiss Supra 55). The surface morphology was examined by white light interferometry (BW-S501, Nikon) The crystalline phases of LLZTO powder and GPEs were characterized by X-ray diffraction (XRD) (D8 ADVANCE, Bruker). The wettability of the Celgard and various GPEs was investigated with a surface contact angle test instrument (Theta Lite, Biolin, Finland). The bending test was performed using a specially designed stepper motor. The thickness of the CNTs film was tested using a digimatic indicator (Mitutoyo, 0.001 mm). Raman spectra were acquired with a LabRAM HR Evolution (Horiba) Raman microscope with a 40× lens and 532 nm excitation lasers. The EIS measurements were carried out using the Autolab (Metrohm).

3. Results and discussion

3.1. Flexible current collectors

Commercial LIBs use Al foil and Cu foil as current collectors for the positive and negative electrodes, respectively. Such metal foils are stiff and subject to fatigue failures and therefore cannot be used in flexible batteries. A current collector for flexible batteries should have superior flexibility, high strength, and high conductivity and should retain its mechanical integrity after undergoing repeated bending. As a promising choice for current collectors in flexible LIBs, the reported research on the carbon material current collectors is still in the laboratory stage, far from the scalable production. For the practical application of flexible LIBs, scalable production of carbon material current collectors is an inevitable requirement. In this work, flexible CNT films which can be scalably prepared are used as current collectors both for the positive and negative electrodes. With a maximum width of 1 m, the mass-produced CNT films can replace Al foil and Cu foil and can be applied to a small LIBs production line to achieve scalable production of flexible LIBs. To understand the mechanical flexibility of the CNTs film, the CNTs film is folded as shown in Fig. 1a. A planar, unfolded CNTs film (30 cm × 30 cm) can be folded up to six times (3.75 cm × 3.75 cm) and still exhibits good flatness, with no obvious creases, demonstrating its superior mechanical flexibility. The SEM image and white light interferometry image of the surface characteristics for the CNTs film are shown in Fig. 1b and c. The surface of the CNTs film is porous, rough and consists of entangled nanotube bundles that form an interconnected network. Fig. 1d shows that the hole depth on the surface of the CNTs film is less than 1 μm, which ensures that the CNTs film has good thickness consistency and can be scalably produced. The roughness and porosity are not found in metal foil, as shown in Fig. S1.

The porous and rough surface of the CNTs film can contribute to increase the contact area between the active material and the current collector, therefore significantly increasing adhesion, as shown in Fig. 2a and b. Fig. 2a and b shows the photographs of flexibility comparison for the LCO cathode coated both on Al foil (LCO/Al foil) and the CNTs film (LCO/CNTs film). The mass loading of the LCO material both on Al foil and CNTs film is ≈5.8 mg/cm^2. As can be seen, the LCO/CNTs film electrode shows more deformable capability than the LCO/Al foil electrode after 1,000 times mechanical bending with a bending radius of 1 mm. No delamination and crack occurred on the LCO/CNTs film but it is clearly shown on LCO/Al foil. Moreover, to further explore the morphological characteristics of the flexible electrodes, cross-sectional SEM images on the region of electrodes under stress were taken, as shown in Fig. 2c and d. Cross-sectional SEM images after bending also show that no cracking or delamination occurs on the LCO/CNTs film (Fig. 2e) but it is clearly shown on LCO/Al foil (Fig. 2f), further demonstrating the superior mechanical flexibility of the flexible electrode when using the CNTs film as the current collector. In addition to the superior flexibility, the rough, porous surface of the CNTs film can increase the contact area with the active material. The other reason for increasing the mechanical flexibility of the electrode is that the deformable capability of the CNTs film is conductive to the embedding and integration of the active material particles through rolling, as shown in Fig. 2e.

To further explore the influence of mass loading on electrode flexibility, the surface and cross-sectional SEM of the LCO/CNTs film with various mass loadings after 1,000 times mechanical bending were carried out and the images are shown in Fig. S2. Although the mass loading of the LCO material increases from 3.6 to 14.0 mg/cm^2, no delamination still occurs on the region of electrodes under stress. However, it must be pointed out that with the increase of

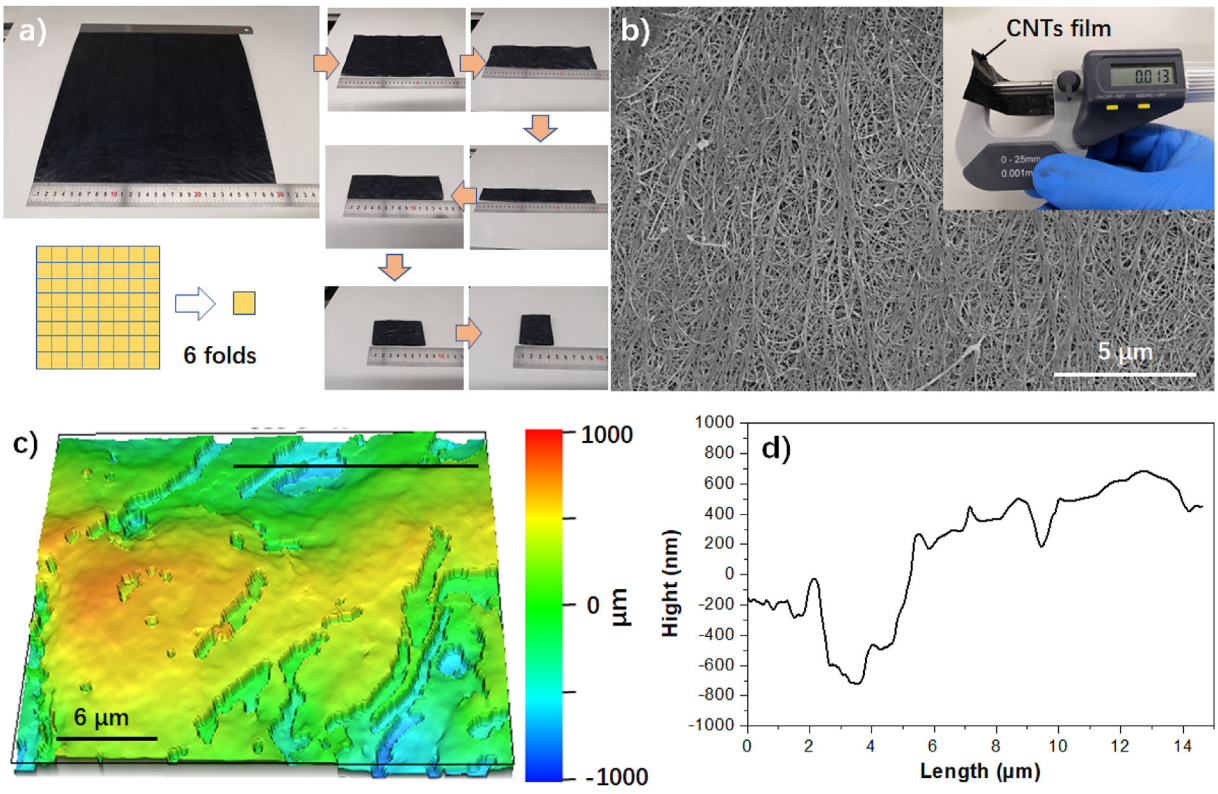

Fig. 1. a) Folding procedures of a CNTs film with six folds. (b) SEM image of the surface morphology of the CNTs film (inset: thickness of the CNTs film). c) White light interferometry image of the CNTs film. d) A profile graph measured along a 15 μm user-drawn black line.

mass loading, cracks in the active material layer become more and more obvious. This is because the higher the mass loading, the thicker the active material layer. Therefore, the flexibility of the active material layer will have a certain decline.

The mechanical strength and deformable capability of the CNTs film, Al foil, and Cu foil were tested and the stress–strain curve is shown in Fig. 3a. The strain of the CNTs film is ~20%, which is much higher than those of Al foil and Cu foil of 2% and 7%, respectively. It is suggested that the CNTs film has excellent deformable capability. The breaking stress of the CNTs film is ~82.1 MPa, just slightly lower than that of Al foil (~108.1 MPa) and Cu foil (~121.6 MPa), but significantly higher than that of most carbon current collectors reported in the literature with the values in the 5–15 MPa range [26,28–30]. For example, Arias et al. reported that the breaking strength and stress of CNTs flexible current collectors are ~9.16 MPa and 0.4%, respectively [26]. Cheng et al. reported a flexible S-carbon nanotubes current collector synthesized by CVD, which can sustain a 10 MPa stress with 9% strain [29]. The increase in tensile strength is due to the fact that the CNTs film is composed of entangled nanotube bundles that form an interconnected network, which is not a feature of other carbon-based materials. The improved CNTs film in this study with high breaking stress and strain is desirable to reduce electrode rupture or cracking during bending, and this also exhibits a high consistency with the SEM images of Fig. 1d–f.

The conductivity of the current collector is closely related to the electrochemical performance of the battery, and the graphitization degree of the CNTs film is also closely related to its electrical conductivity. Therefore, to confirm the graphitization degree of the CNTs film, Raman spectra are tested and displayed in Fig. S3. The group of peaks observed at 1,350 and 1,580 cm^{-1} can be assigned to the disorder-induced phonon mode (D band) and graphite band (G band), respectively [7,44]. The intensity ratio of the D band to the G band (I_D/I_G) is 0.11, demonstrating the high graphitization of the CNTs film. The high graphitization of the CNTs film can contribute to improving its electrical conductivity, and the sheet resistance of the CNTs film is only as low as ~1.4 Ohm/sq, which is far less than most reported current collectors of carbon materials, with the sheet resistance as high as 5–50 Ohm/sq [23–27]. Such enhancement in conductivity will improve the electrochemical performance of flexible batteries when using the CNTs film as the current collector.

Thickness tests are performed at random locations on the CNTs film, Al foil, and Cu foil (inset of Fig. 1b and Table S1). As can be seen, the thickness of the CNTs film is relatively uniform compared to Al foil and Cu foil, and the average thickness is about 13 μm, which shows similar thickness to Al foil (≈16 μm) and Cu foil (≈10 μm). However, the density of the CNTs film is only 0.32 g/cm^{-3}, calculated according to Table S2, which is much lower than the values of Al foil and Cu foil of 2.66 and 8.85 g/cm^{-3}, respectively. The lower density of the CNTs film contributes to the enhancement in gravimetric energy density of LIBs. The gravimetric energy density of the fabricated flexible LCO/LTO electrodes using the CNTs film and metal foil (cathode using Al foil and anode using Cu foil) in different areal capacities is shown in Fig. 3. As can be seen, the gravimetric energy density using the CNTs film is far more than using metal foil.

Therefore, sufficient conductivity, strong adhesion, uniform thickness consistency, strong mechanical flexibility, and scalable production of the CNTs film can meet the requirements of flexible LIBs for current collectors. Moreover, the scalable production of CNT films is compatible with the mainstream industrial production of LIBs.

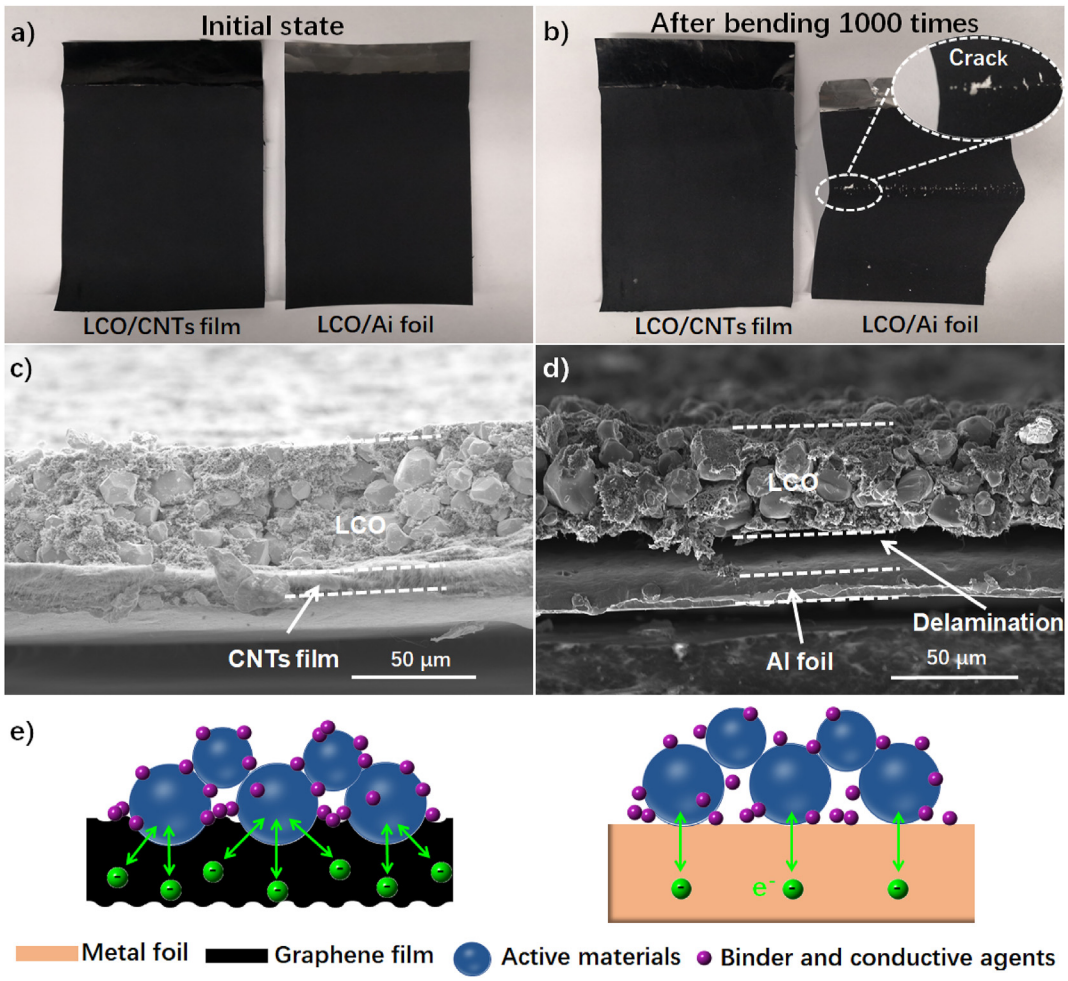

Fig. 2. Photographs of a LCO/CNTs film and LCO/Ai foil a) before and b) after bending 1,000 times and the corresponding (c and d) cross-sectional SEM images. e) Schematic diagram of interface contact between active materials and various current collectors.

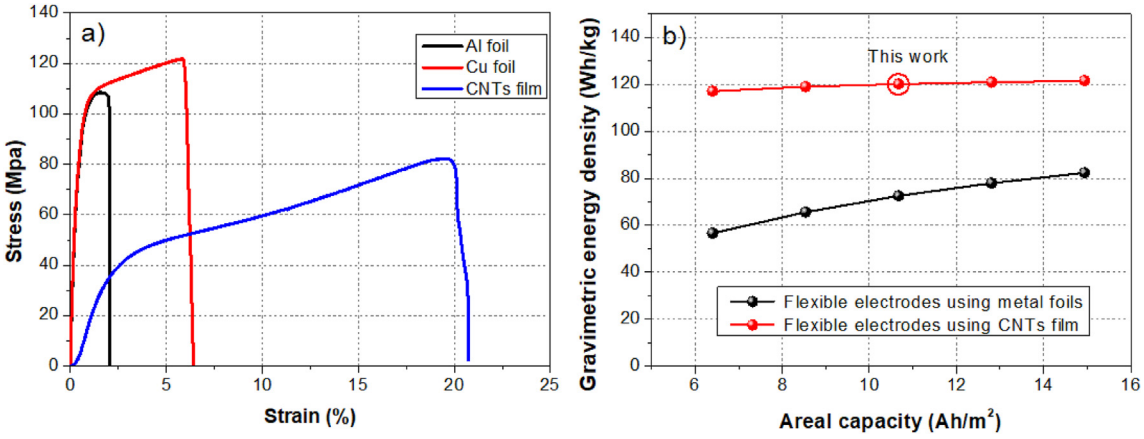

Fig. 3. a) Stress–strain curves of various current collectors. b) The gravimetric energy density of the fabricated flexible LCO/LTO electrodes using the CNTs film and metal foil (cathode using Al foil and anode using Cu foil) in different areal capacities.

3.2. Gel polymer electrolytes

The composite porous GPE consists of the PTC polymer, LLZTO nanoparticle, LiTFSI salt, and liquid electrolyte. A PTC polymeric framework is adopted in the composite porous GPE as the host material, providing high mechanical integrity. The highest dielectric constant of PTC (50–57) compared to previously reported PE (2.3), PP (2.2–2.3), PEO (~5), PAN (5.5), PMMA (3.0), and PVDF (8.15–10.46) is critical to GPE through improving the dissociation degree of $LiPF_6$ [45]. Increasing the dissociation degree of $LiPF_6$ can

obviously increase the ionic conductivity of GPE. Conventional pure polymer GPEs suffer from low ionic conductivity, poor mechanical property, and poor thermal stability. Therefore, a variety of inorganic/organic fillers or plasticizers had been added to enhance their properties [46]. Recently, active fillers (LLZO, LLTO, and LLZTO), which participate in the conduction process, rather than passive fillers (Al_2O_3, SiO_2, TiO_2, $BaTiO_3$, and so on), are preferentially used to fabricate high-conductivity GPEs. In this study, we choose LLZTO as an active filler. LLZTO is one of the most promising solid-state fast Li^+ conductors, exhibiting high ionic conductivity and excellent chemical and thermal stability. To prepare composite porous GPEs with different LLZTO contents, samples with different mass ratios of 0, 5, 15, 25, and 40 wt% (LLZTO/(PTC + LiTFSI + LLZTO)) were prepared and denoted as P-CPE-0%, P-CPE-5%, P-CPE-15%, P-CPE-25%, and P-CPE-40%, respectively (for details, see the experimental section). For comparison, the non-porous composite GPE of PTC/LiTFSI without LLZTO was also fabricated and denoted as N-GPE-0%. As shown in Fig. S4a, the average particle size of nano-LLZTO is about ~500 nm in the SEM images. The XRD patterns of the as-prepared LLZTO, P-GPE-0%, and P-GPE-25% are shown in Fig. S4b. The distinct peaks of LLZTO around 17, 19, 25, 27, 31, and 34° can be indexed to the crystalline phases of the cubic structure (JCPDS no. 80-0457), suggesting the high quality of the LLZTO nanoparticles. When LLZTO and PTC are composited, the patterns of P-GPE-25% contain the peaks of LLZTO and the wide peak of the PTC matrix. In Fig. S5, the EDS mapping images of P-GPE-25% show that La, Zr, and O are evenly distributed, which confirm the uniform distribution of the LLZTO among the GPEs.

In the phase inversion procedure of LLZTO-filled GPEs, the solvent exchange process between DMF and ethanol is good for creating a 3D porous structure for Li^+ migration, and the corresponding SEM images of surface morphology for various GPEs are shown in Fig. 4b–f [47,48]. The cross-sectional SEM images show that the thickness of all GPE membranes is approximately 15 μm. The obtained GPE membranes by the phase inversion procedure can replace a conventional separator and be applied to a small LIBs production line in this study to achieve scalable production of flexible LIBs. The SEM images show many 3D porous structures on the surface and inside of P-GPE-0–40% prepared by the phase inversion method, but not show in N-GPE-0% prepared by the drying method (Fig. 4a).

The 3D porous structure can enhance the wettability of GPEs with liquid electrolytes and promote homogeneous Li^+ distribution. It must be pointed out that when compounded with LLZTO nanoparticles, P-GPE-5–40% demonstrate smaller pores than P-GPE-0%, and the pores become smaller with the increase in the LLZTO content. Since the porous structure is produced by the soluble PTC polymer during the phase inversion procedure, therefore, with the addition of insoluble LLZTO nanoparticles into the PTC host, the porous structure becomes less and the pore size becomes smaller. The smaller porous structure could remarkably enhance the mechanical strength of GPEs. As shown in Fig. S6, P-GPE-40% with the highest LLZTO content exhibits the highest stress of 1.24 MPa, which is higher than P-GPE-0%, P-GPE-5%, P-GPE-15%, and P-GPE-25% with the value of 0.73, 1.08, 1.08, and 1.09 MPa, respectively.

The FTIR spectra of various GPE samples are presented in Fig. 5a. The peak at 880 cm^{-1} is attributed to the vibration of C–C, the peak at 964 cm^{-1} is attributed to the twisting vibration of $-CH_2$, the peak at 1,060 cm^{-1} is attributed to the stretching vibration of C–O, and the peak at 1,170 cm^{-1} is attributed to the vibration of C–F [49,50]. The diffraction peaks of the XRD pattern around 18, 20, and 43° (Fig. S4b) and the peaks of the FTIR spectrum at 811, 835, and 1,236 cm^{-1} indicate the existence of γ-phase PTC in the GPE samples [51]. Moreover, the peak areas of C–C, $-CH_2$, C–O, and C–F gradually decrease with the increase of the LLZTO content. These results indicate that the GPEs have lower crystallinity with the introduction of LLZTO, which can indirectly increase the free-lithium ions and further improve the electrochemical performance of LIBs using composite GPEs. The liquid electrolyte uptake capability correlates strongly to the contact angle. The contact angle results of the various GPEs in Figs. S7 and 5b show that all PTC-based GPEs exhibit a higher contact angle than the Celgard separator at an early stage (t = 10 s), indicating its superior electrolyte wettability to polyethylene (PE), which is the main constituent substrate of the Celgard separator. In all GPEs, P-GPE-25% exhibits the lowest contact angle of 17°. This is because after adding LLZTO ceramic powders into the polymer host, the composite electrolyte/liquid electrolyte interfacial energy decreases [52]. Therefore, as shown in Fig. 5c, P-GPE-25% exhibits the largest electrolyte uptake ratio of 337%, larger than the uptake of the Celgard separator (236%) and P-GPE-0% without LLZTO (321%), respectively.

The effects of morphology, LLZTO percentage, and electrolyte uptake on the ionic conductivity of GPEs are determined by EIS and calculated by Equation (1), and the results are shown in Fig. 5d. It shows that non-porous N-GPE-0% exhibits the lowest ionic conductivity compared to porous P-GPE-0–40%. Moreover, the maximum ionic conductivity of porous GPEs is achieved at the LLZTO content of 25 wt% (P-GPE-25%). The ionic conductivity of P-

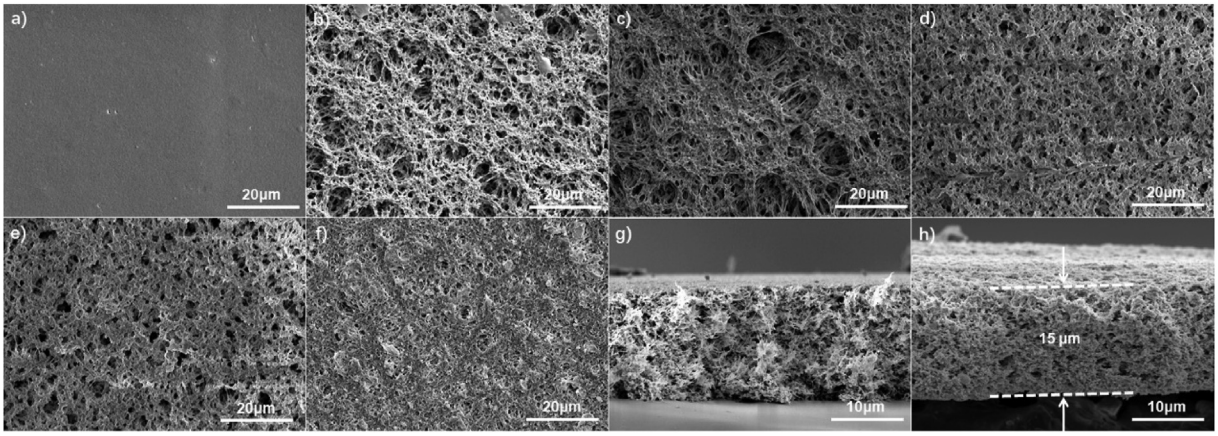

Fig. 4. SEM images of the surface morphology of a) N-GPE-0%, b) P-GPE-0%, c) P-GPE-5%, d) P-GPE-15%, e) P-GPE-25%, and f) P-GPE-40% samples. Cross-sectional SEM images of g) P-GPE-0% and h) P-GPE-25% samples.

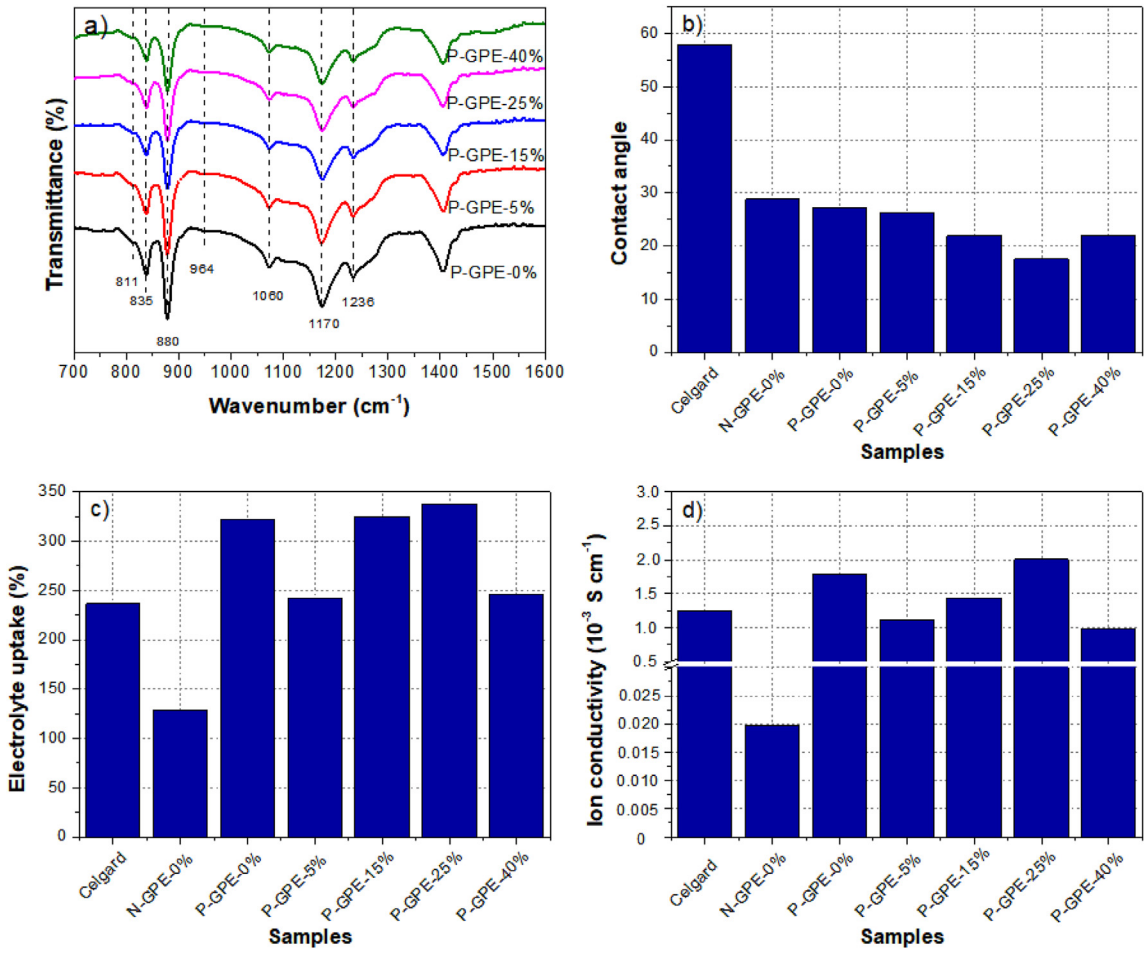

Fig. 5. a) FTIR spectra of various GPEs. b) The contact angle results, c) electrolyte uptake, and d) ionic conductivities of the Celgard separator and various GPEs.

GPE-25% is 2.01 × 10^{-3} S/cm, which is ~102 times higher than that of the non-porous N-GPE-0% and ~1.6 times higher than that of the Celgard separator. However, when the LLZTO content increases to 45 wt%, the ionic conductivity decreases, which may be related with that the excessive aggregation of the LLZTO nano-particles and the decreased contact angle decrease the ionic conductivity of P-GPE-45%. Furthermore, the temperature-dependent ionic conductivities of various GPEs are illustrated in Fig. S8. The ionic conductivities of various GPEs gradually increase as the temperature increases from 25 to 60 °C. P-GPE-25% also exhibits the maximum ionic conductivity among the various GPEs at different temperatures. It reaches 1.8 × 10^{-3} S/cm at 25 °C, 2.2 × 10^{-3} S/cm at 40 °C, and 2.6 × 10^{-3} S/cm at 60 °C. The reasons for the higher ionic conductivity of P-GPE-0–45% than the Celgard separator are: 1) PTC has a high dielectric constant (50–57) than polyethylene of Celgard separator (2.26–2.4) [45,53]. This can generate a large number of charge carriers by effectively dissociating $LiPF_6$ [54]. 2) The porous structure of GPEs contributes to adsorbing more liquid electrolytes and further enabling liquid electrolytes to penetrate into the polymer chains and expand the amorphous polymer into a gel state [55,56]. 3) As a solid-state fast Li^+ conductor, the LLZTO can provide a continuous Li^+ transport channel. 4) The introduction of LLZTO nano-particles can decrease the crystallinity of PTC, thus increasing the segmental mobility of PTC, and further improving the migration of Li ions [57]. 5) Due to the high cation conductivity of LiTFSI, the addition of LiTFSI can increase the fraction of free Li ions and thereby enhance the Li-ions transport [58].

Thermal shrinkage of the GPEs is a vital aspect to evaluate the safety characteristics of the LIBs. SEM images and digital photographs (insets) of the Celgard separator and various GPEs before and after storage at 180 °C for 1 h are shown in Fig. 6. It can be easily found that the Celgard separator suffers a severe shape shrinkage, and the pores disappear due to the hot melting of PE after the thermal treatment. However, although the pore of P-GPE-0% without LLZTO also disappeared after the thermal treatment, the shrinkage rate of the P-GPE-0% membrane is far less than that of the Celgard separator, demonstrating the excellent thermal stability of PTC than PE. However, P-GPE-25% with an LLZTO content of 25 wt% still retains the same shape and pore diameter under the same conditions. Although the treatment time was extended to 3 and 5 h, most of the pores for P-GPE-25% disappeared due to the hot melting of PTC, but only slight shrinkage of the P-GPE-25% membrane occurred (Fig. S9). When the treatment temperature was decreased to 160 °C and the treatment was carried out for 3 and 5 h, the pore diameter and dimension of the P-GPE-25% membrane were stable. The phenomenon reveals that such composite porous electrolytes can effectively eliminate the safety threat caused by internal short-circuit and improve the battery performance under no more than 160 °C.

To further investigate the advantage of the porous GPEs in the cycling stability, Li/Li symmetrical cells with P-GPE-25%, N-GPE-0%, and Celgard separator were assembled, respectively. As shown in Fig. 7, P-GPE-25% delivers long-term cycle stability over 700 h under 0.25 mA/cm^2. The near-constant overpotential is as low as 4 mV. The SEM image of Li foil in Fig. 7c after cycling confirms the

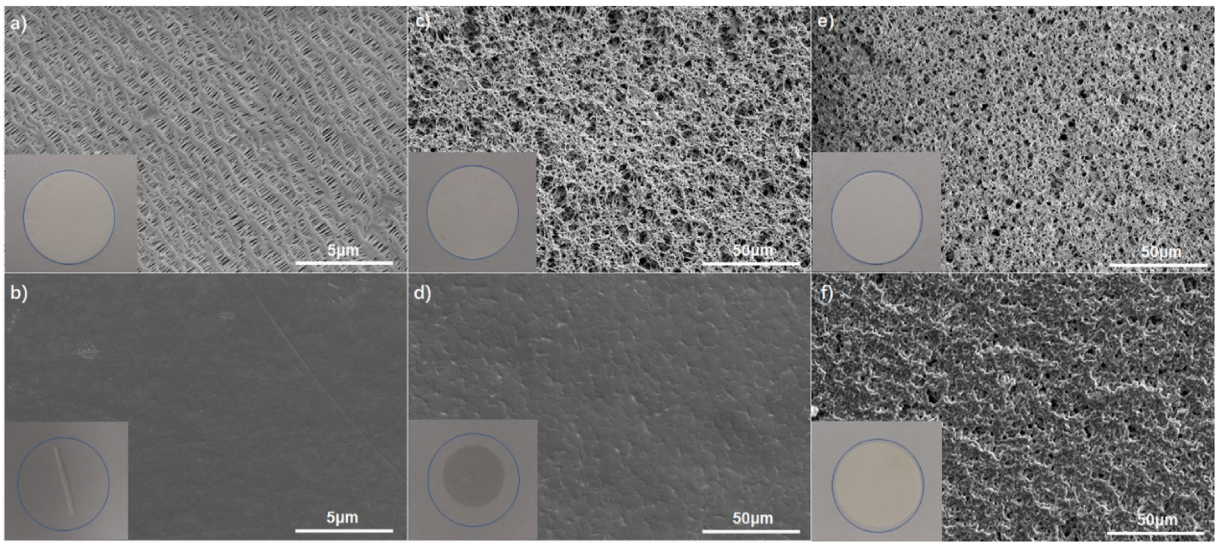

Fig. 6. SEM images of a and b) a commercial Celgard separator, c and d) P-GPE-0%, and e and f) P-GPE-25% before a, c, and e) and after b, d, and f) thermal treatment at 180 °C for 1 h (inset: corresponding photographs).

non-existence of Li dendrite. In contrast, the overpotential of the Celgard separator is initially maintained at ~25 mV for 500 h and gradually increases to over 75 mV after 600 h, and the Li foil after cycling is rougher as compared with those in cells with P-GPE-25% (Fig. 7d). Furthermore, obvious dendrite formation is also observed for N-GPE-0% due to the low ionic conductivity (Fig. 7e). It confirms that P-GPE-25% with high Li^+ diffusivity and interface stability is beneficial for inhibiting lithium dendrites growth.

EIS was used to measure the impedance of Li/Li symmetrical cells with various GPEs at room temperature. Fig. S10 shows the EIS spectra of cells with N-GPE-0%, P-GPE-0%, and P-GPE-25% after 200, 500, and 600 h cycling at 0.25 mA/cm^2, respectively. The EIS spectra consist of two distinct arcs, of which one is in the higher frequency range corresponding to the interfacial resistance of the passivation film R_f, whereas the other is in the lower frequency range corresponding to the charge transfer resistance R_{ct} [59]. The R_f with P-GPE-25% is much lower than those with N-GPE-0% and P-GPE-0%. The interfacial resistances of P-GPE-25% are only 28.1, 34.6, and 57.8 Ω after 200, 500, and 600 h cycling, respectively, indicating the suppressed Li dendrites. In contrast, the R_f with N-GPE-0% significantly increases from 30.4 to 160.2 Ω after 600 h cycling and the R_f with P-GPE-0% also significantly increases from 22.6 to 132.8 Ω after 600 h cycling. The large fluctuations of R_f are consistent with the results of the uneven Li dendrite growth in Fig. 7e.

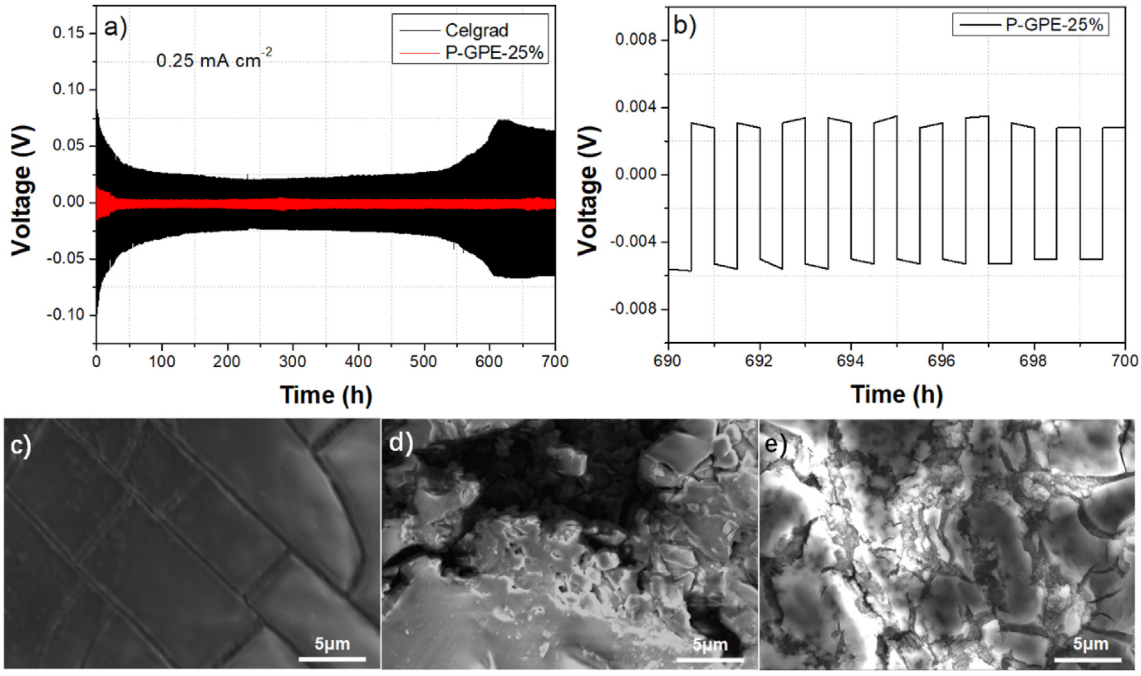

Fig. 7. a and b) Voltage profiles for Li/Li symmetric cells with different separators during galvanostatic cycles under 0.25 mA/cm^2 with 0.5 h stripping and 0.5 h plating alternating steps at 25 °C. SEM images of the Li–metal surface for c) P-GPE-25%, d) Celgard separator, and e) N-GPE-0% cells after 700 h cycling.

3.3. Flexible lithium–ion batteries

The electrochemical study of pouch-type flexible full cells was investigated. All full cell was assembled using LCO as the cathode, LTO as the anode, the CNTs film as the flexible current collector, and various GPEs as the electrolyte and separator. A schematic illustration of the structure of a flexible full cell is presented in Fig. 8a. With the aim to investigate the rate performance of various GPEs at various current densities between 1.5 and 2.8 V, an extended rate performance test from 0.2 to 2 C is conducted and shown in Fig. 8a. It is apparent that the rate performances of all porous GPEs (P-GPE-0% and P-GPE-25%) are better than that of non-porous GPEs (N-GPE-0%) (Fig. 8b). Moreover, the addition of LLZTO will also have significant improvement on the electrochemical performance. Notably, N-GPE-25% exhibits the best rate performance among various GPEs with values of 151.9, 149.4, 142.7, and 132.8 mAh/g for 0.2, 0.5, 1, and 2 C, respectively. When recycled back to 1, 0.5, and 0.2 C, its discharge capacity can still reach 142.7, 147.7, and 150.0 mAh/g, respectively. Furthermore, N-GPE-25% also exhibits the best cycle performance among various GPEs (Fig. 8c). The capacity retention of N-GPE-0%, P-GPE-0%, and P-GPE-25% are 21.3%, 64.6%, and 100% after 200 cycles, respectively. The coulombic efficiency of P-GPE-25% during the cycling process maintains at ~100%. The improved electrochemical performance of P-GPE-25% could be attributed to the improved ionic conductivity of P-GPE-25% and the stable interface between electrodes and GPEs in the cell as presented in Fig. 7c and d.

To investigate the flexibility of the optimum P-GPE-25% full cell (mass loading of LCO: 5.8 mg/cm^2), an in-situ bending test was carried out using a specially designed stepper motor during the charge/discharge cycling. The in-situ bending test was performed at a low speed of 3 mm/s with a bending radius of 1 cm. Bending was carried out approximately 90 times on one electrochemical cycle at 1 C and the charge/discharge curves are shown in Fig. 8d. Overall, there is almost no shift in the charge/discharge curve, indicating an excellent electrochemical stability and mechanical robustness for the flexible full cell. However, when the mass loading of the LCO material is increased to 9.6 and 14.0 mg/cm^2, the polarization of the charge/discharge curves increases significantly, and there is a slight shift in the charge/discharge curves, indicating that the cracks of the active material layer have an adverse effect on the flexibility of the battery (Fig. S11). Moreover, the flexibility of the full cell was further tested by mechanical bending at a speed of 200 mm/s with a bending radius of 1 cm. A charge and discharge cycle was tested at 1 C after every 10,000 times mechanical bending. The discharge-specific capacity of the battery after different bending times is shown in Fig. 8e. The flexible battery could deliver a high discharge initial capacity of 138.3 mAh/g, after

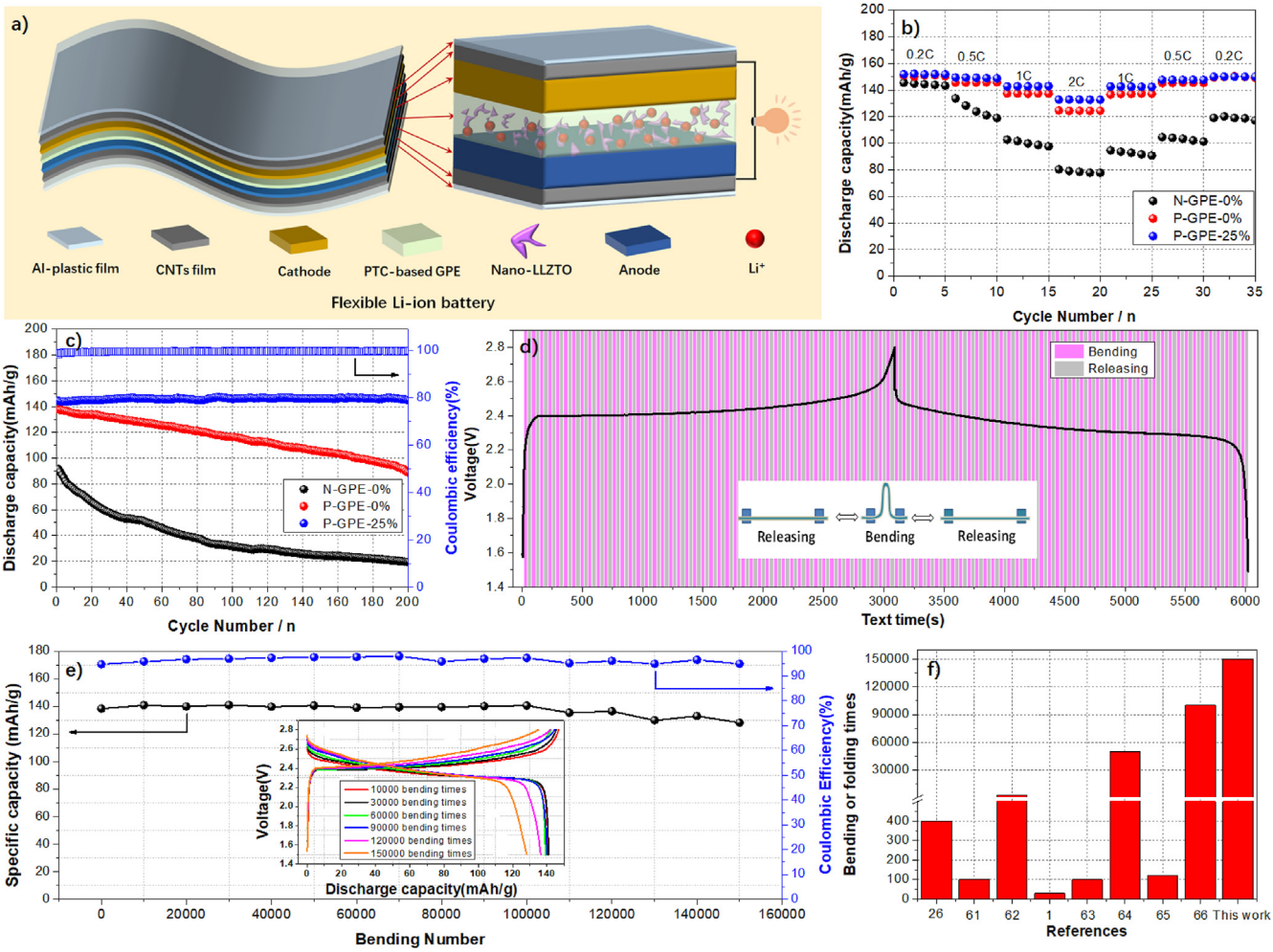

Fig. 8. a) Schematic picture of the flexible Li-ion battery using the CNTs film as a current collector and PTC-based GPE with LLZTO as the electrolyte and separator. b) Rate performance and cycle performance of flexible full cells. c) The charge/discharge curves of a flexible battery with ≈90 times in-situ mechanical bending. e) Cycle performance of the flexible battery cycled at 1 C after different bending times. f) Comparison of bending or folding times between the current work and reported flexible battery.

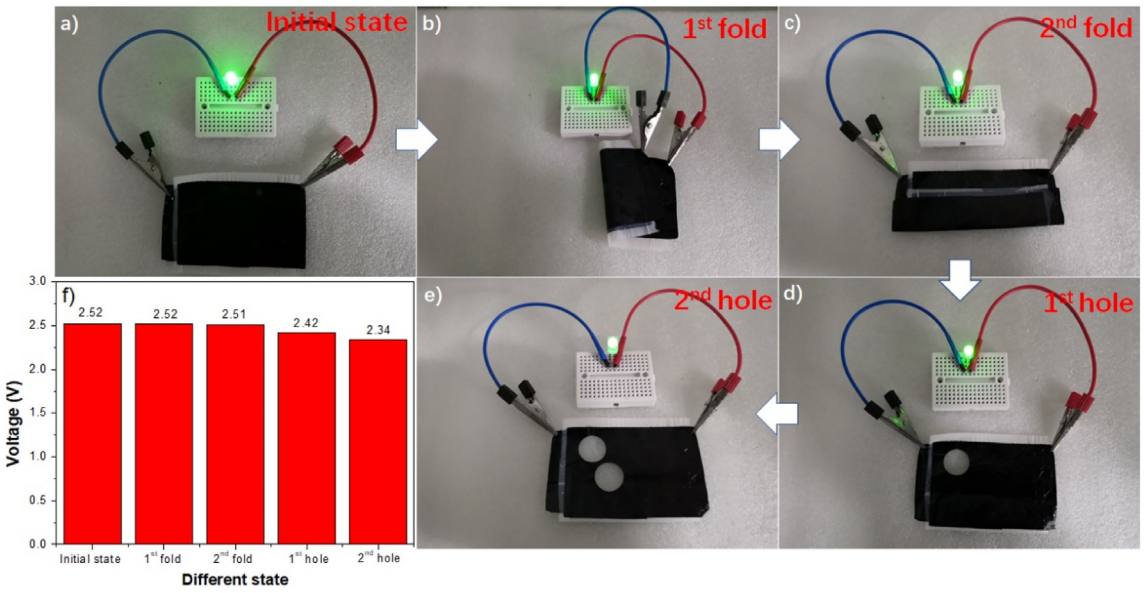

Fig. 9. Folding and punching test for the flexible battery. a) Initial state of the device. b) After the first fold. c) After the second fold. d) After the first punch. e) After the second punch. f) Voltages of the flexible battery under a different status.

150,000 times mechanical bending; its specific capacity can still reach 128.2 mAh/g and only 7% of the initial capacity is lost and it displays the excellent flexibility of the flexible battery. The charge/discharge curves of the flexible full cell maintain stability with little polarization at the 10,000th, 30,000th, 60,000th, 90,000th, and 150,000th bending times (insets of Fig. 8e). The comparison of bending or folding times with literature reports is exhibited in Fig. 8f [1,26,60–65]. Moreover, the comparison of more detailed information is exhibited in Table S3. Upon comparison with the literature reports, it was found that flexible batteries that could bend so many times have not been reported.

Unlike conventional coin, column, or square-shaped batteries, which are intolerant to any damages, the flexible battery can be tailored to any desired shape to meet the demands of high-level integration and wearability. It is very impressive that the unpackaged flexible battery was still able to power a green light-emitting diode (LED) after folding and punching a few times. (Fig. 9a–e). It is noteworthy that the open voltage of the flexible battery remained at 2.34 V, over 92.8% of the initial value, demonstrating an ignorable current leakage during folding and punching. These results demonstrate that the flexible battery can serve as a reliable and tailorable energy storage unit that can be shaped as required to cater to future wearable applications.

4. Conclusions

In summary, we successfully fabricated a safety-reinforced flexible and foldable LIB for future scalable production. The flexible battery uses $LiCoO_2$ as the cathode, $Li_4Ti_5O_{12}$ as the anode, a CNTs film as the flexible current collector, and a novel porous composite gel polymer electrolyte as the electrolyte and separator. The flexible CNTs film that can be fabricated on a large scale is ultrathin and ultra-light, with a high mechanical strength and a high electrical conductivity, and it can be repeatedly bent tens of thousands of times without plastic deformation. The rough and porous surface characteristics of the CNTs film can contribute to increasing the contact area between the active material and the current collector, therefore significantly increasing adhesion and avoiding cracking or delamination. More importantly, the thin CNTs film minimizes the thickness of inactive components within the battery and also enhances the gravimetric energy density 1.6 times higher than those from the standard battery using metal current collectors. In addition, benefiting from the porous structure and compositing with LLZTO and LiTFSI, the as-prepared PTC-based GPEs exhibit a high ionic conductivity and superior thermal and electrochemical stabilities and therefore effectively prevent Li-dendrite propagation. As a result, the flexible LIB using the CNTs film and porous composite GPE in this study presents excellent flexibility, good rate, and cycle performance. More importantly, excellent safety characteristic is obtained even under extremely severe conditions, such as repeated folding and punching. This work not only exhibits the solution for flexible energy storage devices but also provides a new platform for the scalable applications of flexible and wearable energy storage technologies.

Data availability

The data that support the findings of this study are available from the corresponding author upon reasonable request.

CRediT authorship contribution statement

W. Shen and T. Xu: Conceptualization, Methodology, Writing – Original Draft. K. Li, L. Yang and Y. Zhou: Validation. M. Zhong and F. Yang: Resources. X. Xu: Project administration. Y. Wang: Software.Y. Zhang, Q. Li, Z. Yong, M. Zheng, H. Li and Q. Wang: Methodology. D. Wei: Conceptualization, Funding acquisition, Project administration.

Declaration of competing interest

The authors declare that they have no known competing financial interests or personal relationships that could have appeared to influence the work reported in this paper.

Acknowledgments

W. Shen and T. Xu contributed equally to this work. This work was supported by Beijing Municipal Science and Technology Commission No. Z181100004818004, No. Z181100001018029 and No. Z191100006119027. The authors also appreciate the technical assistance from the BGI Characterization & Quality Assurance Center.

Appendix A. Supplementary data

Supplementary data to this article can be found online at https://doi.org/10.1016/j.mtener.2021.100889.

References

[1] X. Pu, L. Li, H. Song, C. Du, Z. Zhao, C. Jiang, G. Cao, W. Hu, Z. Wang, A self-charging power unit by integration of a textile triboelectric nanogenerator and a flexible lithium-ion battery for wearable electronics, Adv. Mater. 27 (2015) 2472–2478.
[2] T. Liu, M. Zhang, Y. Wang, Q. Wang, C. Lv, K. Liu, S. Suresh, Y. Yin, Y. Hu, Y. Li, X. Liu, S. Zhong, B. Xia, Z. Wu, Engineering the surface/interface of horizontally oriented carbon nanotube macrofilm for foldable lithium-ion battery withstanding variable weather, Adv. Energy Mater. 8 (2018) 1802349.
[3] J. Hu, Z. Wu, S. Zhong, W. Zhang, S. Suresh, A. Mehta, N. Koratkar, Folding insensitive, high energy density lithium-ion battery featuring carbon nanotube current collectors, Carbon 87 (2015) 292–298.
[4] Y. Zhang, Y. Jiao, M. Liao, B. Wang, H. Peng, Carbon nanomaterials for flexible lithium ion batteries, Carbon 124 (2017) 79–88.
[5] J. Ren, L. Li, C. Chen, X. Chen, Z. Cai, L. Qiu, Y. Wang, X. Zhu, H. Peng, Twisting carbon nanotube fibers for both wire-shaped micro-supercapacitor and micro-battery, Adv. Mater. 25 (2013) 1155–1159.
[6] J. Zhang, Q. Li, C. Ouyang, X. Yu, M. Ge, X. Huang, E. Hu, C. Ma, S. Li, R. Xiao, W. Yang, Y. Chu, Y. Liu, H. Yu, X. Yang, X. Huang, L. Chen, H. Li, Trace doping of multiple elements enables stable battery cycling of $LiCoO_2$ at 4.6 V, Nat. Energy 4 (2019) 594–603.
[7] W. Shen, H. Li, Z. Guo, C. Wang, Z. Li, Q. Xu, H. Liu, Y. Wang, Y. Xia, Double-nanocarbon synergistically modified $Na_3V_2(PO_4)_3$: an advanced cathode for high-rate and long-life sodium-ion batteries, ACS Appl. Mater. Interfaces 8 (2016) 15341–15351.
[8] W. Shen, H. Li, Z. Guo, Z. Li, Q. Xu, H. Liu, Y. Wang, Improvement on the high-rate performance of Mn-doped $Na_3V_2(PO_4)_3$/C as a cathode material for sodium ion batteries, RSC Adv. 6 (2016) 71581–71588.
[9] W. Shen, H. Li, C. Wang, Z. Li, Q. Xu, H. Liu, Y. Wang, Improved electrochemical performance of the $Na_3V_2(PO_4)_3$ cathode by B-doping of the carbon coating layer for sodium-ion batteries, J. Mater. Chem. A 3 (2015) 15190–15201.
[10] H. Gwon, H. Kim, K. Lee, D. Seo, Y. Park, Y. Lee, B. Ahn, K. Kang, Flexible energy storage devices based on graphene paper, Energy Environ. Sci. 4 (2011) 1277–1283.
[11] G. Zhou, F. Li, H. Cheng, Progress in flexible lithium batteries and future prospects, Energy Environ. Sci. 7 (2014) 1307–1338.
[12] Q. Wang, S. Zhong, J. Hu, T. Liu, X. Zhu, J. Chen, Y. Hong, Z. Wu, Potential threshold of anode materials for foldable lithium-ion batteries featuring carbon nanotube current collectors, J. Power Sources 310 (2016) 70–78.
[13] D. Wei, P. Hiralal, H. Wang, H. Unalan, M. Rouvala, I. Alexandrou, P. Andrew, T. Ryhänen, G. Amaratunga, Hierarchically structured nanocarbon electrodes for flexible solid lithium batteries, Nano Energy 2 (2013) 1054–1062.
[14] F. Bonaccorso, L. Colombo, G. Yu, M. Stoller, V. Tozzini, A. Ferrari, R. Ruoff, V. Pellegrini, Graphene, related two-dimensional crystals, and hybrid systems for energy conversion and storage, Science 347 (2015) 1246501.
[15] S. Chew, S. Ng, J. Wang, P. Novák, F. Krumeich, L. Shu, J. Chen, K. Hua, Flexible free-standing carbon nanotube films for model lithium-ion batteries, Carbon 47 (2009) 2976–2983.
[16] S. Lee, B. Gallant, Y. Lee, N. Yoshida, Y. Dong, Y. Yamada, S. Noda, A. Yamada, S. Yang, Self-standing positive electrodes of oxidized few-walled carbon nanotubes for light-weight and high-power lithium batteries, Energy Environ. Sci. 5 (2012) 5437–5444.
[17] J. Chen, A. Minett, Y. Liu, C. Lynam, P. Sherrell, C. Wang, G. Wallace, Direct growth of flexible carbon nanotube electrodes, Adv. Mater. 20 (2008) 566–570.
[18] G. Zhou, D. Wang, P. Hou, W. Li, N. Li, C. Liu, F. Li, H. Cheng, A nanosized Fe_2O_3 decorated single-walled carbon nanotube membrane as a high-performance flexible anode for lithium ion batteries, J. Mater. Chem. 22 (2012) 17942–17946.
[19] H. Zhang, C. Feng, Y. Zhai, K. Jiang, Q. Li, S. Fan, Cross-stacked carbon nanotube sheets uniformly loaded with SnO_2 nanoparticles: a novel binder-free and high-capacity anode material for lithium-ion batteries, Adv. Mater. 21 (2009) 2299–2304.
[20] K. Wang, S. Luo, Y. Wu, X. He, F. Zhao, J. Wang, K. Jiang, S. Fan, Super-aligned carbon nanotube films as current collectors for lightweight and flexible lithium ion batteries, Adv. Funct. Mater. 23 (2013) 846–853.
[21] L. Cui, L. Hu, J. Choi, Y. Cui, Light-weight free-standing carbon nanotube-silicon films for anodes of lithium ion batteries, ACS Nano 4 (2010) 3671–3678.
[22] Y. Song, Y. Jiang, L. Shi, S. Cao, X. Feng, M. Miao, J. Fang, Solution-processed assembly of ultrathin transparent conductive cellulose nanopaper embedding AgNWs, Nanoscale 7 (2015) 13694–13701.
[23] W. Wang, Q. Xu, H. Liu, Y. Wang, Y. Xia, A flexible symmetric sodium full cell constructed using the bipolar material $Na_3V_2(PO_4)_3$, J. Mater. Chem. A 5 (2017) 8440–8450.
[24] L. Hu, H. Wu, F. Mantia, Y. Yang, Y. Cui, Thin, flexible secondary Li-ion paper batteries, ACS Nano 4 (2010) 5843–5848.
[25] A. Gaikwad, D. Steingart, T. Ng, D. Schwartz, G. Whiting, A flexible high potential printed battery for powering printed electronics, Appl. Phys. Lett. 102 (2013) 233302.
[26] A. Gaikwad, B. Khau, G. Davies, B. Hertzberg, D. Steingart, A. Arias, A high areal capacity flexible lithium-ion battery with a strain-compliant design, Adv. Energy Mater. 5 (2015) 1401389.
[27] L. Hu, J. Choi, Y. Yang, S. Jeong, L. Mantia, Fabio, L. Cui, Y. Cui, Highly conductive paper for energy-storage devices, Proc. Natl. Acad. Sci. U. S. A. 106 (2009) 21490–21494.
[28] S. Liu, Z. Wang, Y. Chang, B. Hao, W. Xiong, A flexible TiO(B)-based battery electrode with superior power rate and ultralong cycle life, Adv. Mater. 25 (2013) 3462–3467.
[29] G. Zhou, D. Wang, F. Li, P. Hou, L. Yin, C. Liu, G. Lu, I. Gentle, H. Cheng, A flexible nanostructured sulphur-carbon nanotube cathode with high rate performance for Li-S batteries, Energy Environ. Sci. 5 (2012) 8901–8906.
[30] Y. Cheng, S. Lu, H. Zhang, C. Varanasi, J. Liu, Synergistic effects from graphene and carbon nanotubes enable flexible and robust electrodes for high-performance supercapacitors, Nano Lett. 12 (2012) 4206–4211.
[31] M. Park, I. Choi, J. Hong, O. Kim, Polymer electrolytes integrated with ionic liquids for future electrochemical devices, J. Appl. Polym. Sci. 129 (2013) 2363–2376.
[32] J. Kalhoff, G. Eshetu, D. Bresser, S. Passerini, Safer electrolytes for lithium-ion batteries: state of the art and perspectives, Chemsuschem 8 (2015) 2154–2175.
[33] T. Shi, Y. Ji, Z. Zhang, Y. Yang, Recent progress in research on high-voltage electrolytes for lithium-ion batteries, ChemPhysChem 15 (2014) 1956–1969.
[34] J. Zhang, B. Sun, X. Huang, S. Chen, G. Wang, Honeycomb-like porous gel polymer electrolyte membrane for lithium ion batteries with enhanced safety, Sci. Rep. 4 (2014) 6007.
[35] A. Arya, A.L. Sharma, Polymer electrolytes for lithium ion batteries: a critical study, Ionics 23 (2017) 497–540.
[36] L. Porcarelli, C. Gerbaldi, F. Bella, J.R. Nair, Super soft all-ethylene oxide polymer electrolyte for safe all-solid lithium batteries, Sci. Rep. 6 (2016) 19892.
[37] Y. Shi, B. Wang, Mechanical properties of carbon fiber/cellulose composite papers modified by hot-melting fibers, Prog. Nat. Sci. 24 (2014) 56–60.
[38] Y. Wang, K. Chen, Low-cost, lightweight electrodes based on carbon fibers as current collectors for aluminum-ion batteries, J. Electroanal. Chem. 849 (2019) 113374.
[39] H. Lu, J. Hagberg, G. Lindbergh, A. Cornell, $Li_4Ti_5O_{12}$ flexible, lightweight electrodes based on cellulose nanofibrils as binder and carbon fibers as current collectors for Li-ion batteries, Nano Energy 39 (2017) 140–150.
[40] J. Shi, H. Peng, L. Zhu, W. Zhu, Q. Zhang, Template growth of porous graphene microspheres on layered double oxide catalysts and their applications in lithium–sulfur batteries, Carbon 92 (2015) 96–105.
[41] J. Cao, C. Chen, Q. Zhao, N. Zhang, Q. Lu, X. Wang, Z. Niu, J. Chen, A flexible nanostructured paper of a reduced graphene oxide-sulfur composite for high-performance lithium-sulfur batteries with unconventional configurations, Adv. Mater. 28 (2016) 9629–9636.
[42] C. Yan, T. Song, X. Lu, J. Wu, Flexible carbon nanotube-graphene/sulfur composite film: free-standing cathode for high-performance lithium/sulfur batteries, J. Phys. Chem. C 119 (2015) 10288–10294.
[43] X. Ye, Q. Zhou, C. Jia, Z. Tang, Z. Wan, X. Wu, A knittable fibriform supercapacitor based on natural cotton thread coated with graphene and carbon nanoparticles, Electrochim. Acta 206 (2016) 155–164.
[44] W. Shen, C. Wang, Q. Xu, H. Liu, Y. Wang, Nitrogen-doping-induced defects of a carbon coating layer facilitate Na-storage in electrode materials, Adv. Energy Mater. 5 (2015) 1400982.
[45] S. Yang, R. Benitez, A. Fuentes, K. Lozano, Dielectric analysis of VGCNF reinforced polyethylene composites, Compos. Sci. Technol. 67 (2007) 1159–1166.
[46] S. Thayumanasundaram, V.S. Rangasamy, W.S. Jin, J.P. Locquet, Lithium polymer electrolytes based on sulfonated poly (ether ether ketone) for lithium polymer batteries, Eur. J. Inorg. Chem. 2015 (2015) 5395–5404.
[47] X. Gao, Q. Sun, X. Yang, J. Liang, A. Koo, W. Li, J. Liang, J. Wang, R. Li, F. Holness, A. Price, S. Yang, T. Sham, X. Sun, Toward a remarkable Li-S battery via 3D printing, Nano Energy 56 (2019) 595–603.
[48] J. Mandal, Y. Fu, A. Overvig, M. Jia, K. Sun, N. Shi, H. Zhou, X. Xiao, N. Yu, Y. Yang, Hierarchically porous polymer coatings for highly efficient passive daytime radiative cooling, Science 362 (2018) 315–319.
[49] B. Li, Q. Su, L. Yu, D. Wang, B. Xu, $Li_{0.35}La_{0.55}TiO_3$ nanofibers enhanced poly(vinylidene fluoride)-based composite polymer electrolytes for all-solid-state batteries, ACS Appl. Mater. Interfaces 11 (2019) 42206–42213.
[50] Zhuang Hua, Ma Wencheng, Xie Jingwei, Liu Xiaoyu, Li Bobo, Jiang Yong, Huang Shoushuang, Chen Zhiwen, Zhao Bing, Solvent-free synthesis of PEO/

garnet composite electrolyte for high-safety all-solid-state lithium batteries, J. Alloy. Compd. 860 (2020) 157915.
[51] Z. Xue, T. Liu, S. Zhang, H. Xin, B. Xu, Y. Lin, B. Xu, L. Li, C. Nan, S. Yang, Synergistic coupling between $Li_{6.75}La_3Zr_{1.75}Ta_{0.25}O_{12}$ and poly(vinylidene fluoride) induces high ionic conductivity, mechanical strength, and thermal stability of solid composite electrolytes, J. Am. Chem. Soc. 139 (2017) 13779–13785.
[52] X. Shi, Q. Sun, B. Boateng, Y. Niu, Y. Han, W. Lv, W. He, A quasi-solid composite separator with high ductility for safe and high-performance lithium-ion batteries, J. Power Sources 414 (2019) 225–232.
[53] S. Zhang, N. Zhang, C. Huang, K. Ren, Q. Zhang, Microstructure and electromechanical properties of carbon nanotube/poly (vinylidene fluoride-trifluoroethylene-chlorofluoroethylene) composites, Adv. Mater. 17 (2005) 1897–1901.
[54] C. Chiang, Y. Shen, M. Reddy, P. Chu, Complexation of poly(vinylidene fluoride):$LiPF_6$ solid polymer electrolyte with enhanced ion conduction in 'wet' form, J. Power Sources 123 (2003) 222–229.
[55] Y. Saito, H. Kataoka, E. Quartarone, P. Mustarelli, Carrier migration mechanism of physically cross-linked polymer gel electrolytes based on PVDF membranes, J. Phys. Chem. B 106 (2002) 7200–7204.
[56] Z. Cui, Y. Xu, L. Zhu, J. Wang, Z. Xi, B. Zhu, Preparation of PVDF/PEO-PPO-PEO blend microporous membranes for lithium ion batteries via thermally induced phase separation process, J. Membr. Sci. 325 (2008) 957–963.
[57] B. Li, Q. Su, L. Yu, D. Wang, S. Ding, M. Zhang, G. Du, B. Xu, $Li_{0.35}La_{0.55}TiO_3$ nanofibers enhanced poly(vinylidene fluoride)-based composite polymer electrolytes for all-solid-state batteries, ACS Appl. Mater. Interfaces 11 (2019) 42206–42213.
[58] W. Zhou, Z. Wang, Y. Pu, Y. Li, S. Xin, X. Li, J. Chen, J. Goodenough, Double-layer polymer electrolyte for high-voltage all-solid-state rechargeable batteries, Adv. Mater. 31 (2019) 1805574.
[59] H. Huo, X. Li, Y. Chen, J. Liang, S. Deng, X. Gao, K. Doyle-Davis, R. Li, X. Guo, Y. Shen, C.-W. Nan, X. Sun, Bifunctional composite separator with a solid-state-battery strategy for dendrite-free lithium metal batteries, Energy Storage Mater. 29 (2020) 361–366.
[60] S. Xu, Y. Zhang, J. Cho, J. Lee, X. Huang, L. Jia, J. Fan, Y. Su, J. Su, H. Zhang, H. Cheng, B. Lu, C. Yu, C. Chuang, T. Kim, T. Song, K. Shigeta, S. Kang, C. Dagdeviren, I. Petrov, P. Braun, Y. Huang, U. Paik, J. Rogers, Stretchable batteries with self-similar serpentine interconnects and integrated wireless recharging systems, Nat. Commun. 4 (2013) 1543.
[61] M. Park, M. Noh, S. Lee, M. Ko, J. Cho, Flexible high-energy Li-ion batteries with fast-charging capability, Nano Lett. 14 (2014) 4083–4089.
[62] Y. Ding, H. Ren, Y. Huang, F. Chang, P. Zhang, Three-dimensional graphene/$LiFePO_4$ nanostructures as cathode materials for flexible lithium-ion batteries, Mater. Res. Bull. 48 (2013) 3713–3716.
[63] G. Zhou, L. Li, D. Wang, X. Shan, S. Pei, F. Li, H. Cheng, A flexible sulfur-graphene-polypropylene separator integrated electrode for advanced Li-S batteries, Adv. Mater. 27 (2015) 641–647.
[64] B. Liu, J. Zhang, X. Wang, G. Chen, D. Chen, C. Zhou, G. Shen, Hierarchical three-dimensional $ZnCo_2O_4$ nanowire arrays/carbon cloth anodes for a novel class of high-performance flexible lithium-ion batteries, Nano Lett. 12 (2012) 3005–3011.
[65] W. Shen, K. Li, Y. Lv, T. Xu, D. Wei, Z. Liu, Highly-safe and ultra-stable all-flexible gel polymer lithium ion batteries aiming for scalable applications, Adv. Energy Mater. 10 (2020) 1904281.